Tellus (2003), 55B, 879–892
Printed in UK. All rights reserved

TELLUS
ISSN 0280–6509

CO_2 flux measurements in Russian Far East tundra using eddy covariance and closed chamber techniques

By D. G. ZAMOLODCHIKOV[1]*, D. V. KARELIN[1,2], A. I. IVASCHENKO[2], W. C. OECHEL[3] and S. J. HASTINGS[3], [1]*Forest Ecology and Production Center, Russian Academy of Sciences, Profsoyuznaya 84/32, Moscow 117810, Russia;* [2]*Biological Department, Moscow State University, Vorobyovy gory, Moscow 119899, Russia;* [3]*San Diego State University, 5500 Campanille Drive, San Diego, CA 92182, USA*

(Manuscript received 15 January 2002; in final form 11 March 2003)

ABSTRACT

The objective of this study was to estimate the CO_2 exchange of a tundra ecosystem in the Russian Far East using the eddy covariance technique using closed-chamber measurements as a reference. An eddy covariance tower was placed near the Lavrentiya settlement (Chukotskiy Peninsula, Russia, 65° 36′N, 171°04′W) within a typical tundra landscape. During the 85 d of continuous measurements [Julian days (JD) 205–289, 2000] the CO_2 exchange of the studied ecosystem was found to be close to equilibrium (a carbon sink at 10.2 gC m^{-2}). In the late summer period (JD 205–240) the ecosystem sequestered 32.1 gC m^{-2}, whereas in autumn (JD 241–289), it was functioning as a carbon source of 21.9 gC m^{-2}. Model-based estimates of ecosystem respiration and gross primary production were obtained over the period of observations. These are the first eddy covariance-based measurements performed in the Russian tundra.

1. Introduction

Arctic ecosystems accumulate large amounts of organic carbon in the permafrost, soils and plant canopy (Billings, 1987; Melillo et al., 1993) and make significant contributions to the global carbon budget. Their importance is highlighted by the observable variation in seasonal atmospheric changes in the Northern regions that coincide with peak season CO_2 drawdown and autumn respiration in Arctic regions (Zamolodchikov and Karelin, 2001; Zimov et al., 1999). The Arctic ecosystems have been shown to acclimate rapidly to the gradual changes in temperature. As the environmental conditions become warmer and drier, the gross respiration in tundra and forest–tundra ecosystems tends to outpace the gross production, which causes these ecosystems to act as a source rather than sink of the atmospheric carbon. This natural phenomenon was observed in the 1980s and early 1990s in Alaska (Oechel et al.; 1993, 1995; Oechel and Vourlitis, 1994) and East Siberia (Zimov et al., 1993; 1996). In the late 1990s, the Alaskan tundra reverted to a summer carbon sink despite continuing warming and drying (Oechel et al., 2000a). These data underline the sensitivity of the cold, permafrost laden Arctic ecosystems to Global Change and in particular, changes in temperature (Oechel and Vourlitis, 1994).

Understanding the present contribution of the Arctic to the global budget of greenhouse gases is complicated by the fact that warming is not uniformally observed for all of the Arctic (Chapman and Walsh, 1993). Hence, it is critical to include varied sites in order to accurately estimate the Arctic ecosystems response to warming and possible changes in ecosystem functioning. The Bering Sea region, also called Beringia, serves as a good example as it includes Arctic and subarctic territories of Central and Western Alaska (USA) to the east, and the Chukotskiy Peninsula to the west from the Bering Strait. These neighboring regions were connected in the geological past, and presently have similar relief and vegetation cover,

*Corresponding author.
e-mail: dzamolod@cepl.rssi.ru

but vary in the climate history over the last decades. Since the 1960s, the climate of the Alaskan Arctic demonstrated an apparent trend to warming (Oechel et al., 2000a), while the Chukotskiy peninsula exhibited no significant trend in the air temperature (Zukert and Zamolodchikov, 1997). Hence, an understanding of the response of Beringia system to climate changes requires representative, region-scale information on greenhouse gas fluxes.

Currently, micrometeorological methods are considered to be the most reliable and practicable for long-term measurements of ecosystem carbon flux (Baldocchi et al., 1988; 1996; Oechel et al., 2000a) and are of wide use worldwide (Lafleur, 1999; Miyata et al., 2000; Rannik et al., 2000 etc.). Whereas there are a number of permanent micrometeorological sites (Harazono et al., 1998; Oechel et al., 2000a; Vourlitis and Oechel, 1997) as well as seasonal estimates (Eugster et al., 1997; Williams et al., 2000) in Alaska, no such studies have been undertaken in the Russian Arctic. The purpose of this survey is to estimate the recent pattern and main ecological controls of net CO_2 exchange of tundra ecosystems in the Russian portion of Beringia.

2. Materials and methods

2.1. Field site location

A micrometeorological tower was placed near the village of Lavrentiya, 3.5 km from the nearest building and 2 km to the west of the Bering Sea coastline (65° 36′N, 171°04′W). The sampling area is located on a gentle slope of eastern exposure, between the *golets* (bald peak) mountain zone and a plain sea terrace. The elevation varies between 300–700 m a.s.l. with gently sloping ridges (5–10°) and hills separated by river and stream valleys and small shallow lakes, which is characteristic of post-glacier relief (Kozhevnikov and Zheleznov-Chukotskii, 1995). The area is part of the zone of continuous permafrost, however, unlike the inner, more continental regions of the peninsula, the coastal areas are exposed to a monsoon-like climate, which is controlled by air mass circulation over the Pacific and Arctic Oceans. Marine winds, predominant in the coastal regions, cause cloudy weather and frequent fogs during the warm season. According to the stationary, long-term (1951–1985) observations at Lavrentiya weather station (*Scientific-applied reference book on the climate of the USSR*, 1990), the mean annual air temperature is −5.8 °C, one of the highest in the entire Eurasian tundra zone. The mean air temperature in the warmest month, July, is 8.1 °C, while in the coldest month, February, it is -−18.7 °C. The absolute maximum summer air temperature never exceeds 26 °C, and minimal winter temperature may fall as low as −42 °C. The maximum and minimum monthly wind speed is 8.3 m s^{-1} (February) and 3.8 m s^{-1} (June/July), respectively. Mean annual precipitation is one of the highest in the Russian tundra (580 mm).

The site is located within a typical tundra landscape of the Russian Far East region. Two main habitats were mesic microelevations (uplands or hummocks) with corresponding microdepressions (lowlands or hollows), and waterlogged sedge ecosystems (*Carex–Eriophorum* lowlands). Elevated mesic microhabitats are dominated by *Salix pulchra, Betula exilis, Ledum decumbens, Vaccinium vitis-ideae, V. uliginosum* and *Empetrum hermafroditum*. A well developed understory is represented by mosses (*Decranum* spp., *Polytrichum* spp.) and fruticose lichens (*Thamnolia vermicularis, Dactylina arctica, Peltigera* spp, *Cladonia* spp *and Cetraria* spp.), while wetter microdepressions are dominated by *Eriophorum vaginatum* and *Carex stans* with *Salix pulchra* in the understory. Bog mosses (*Sphagnum* spp.) and feather mosses (*Aulacomnium tirgidum, Hylocomium alascanum, Ptilidium ciliare* and others) are poorly developed. Waterlogged sedge habitats occupy areas of seasonal run-off and are overgrown with a dense sedge canopy of *Eriophorum polystachyon (angustifolium)* and *Carex stans*. The moss layer of *Sphagnum* spp. is normally submerged and oppressed.

The microelevations are developed on automorphic, acidic, loamy permafrost soils. Peaty–gley, waterlogged permafrost soils are characteristic of wet lowland habitats. In general, the local soils can be classified as loamy variant of Gley–Histic Cryosols.

As it is follows from micrometeorological theory, the most reliable results of turbulent flux measurements can be obtained when the slope of the terrain (instrumentation footprint) is less than 8–15° (Baldocchi et al., 1988). In our case, the micrometeorological eddy covariance tower was located on a gentle slope of 4.3° in the East–West, and of 2.2° in the South–North direction. Surface roughness and vegetation homogeneity are two other important characteristics. The average vertical difference between the elevated and lowered microrelief elements within the studied site is only about 15 cm. The developed vascular plant canopy was 20–25 cm in height in

microdepressions and 10–15 cm in microelevations; in other words, surface roughness decreases as plant growth increases. A horizontal variability of the studied forms of microrelief is 0.2–2 m. No lakes, rivers or considerable bare ground patches were located within the instrumentation footprint. Hence the studied site meets all needed requirements to apply the eddy covariance technique (Baldocchi et al., 1988).

2.2. *Sampling methods*

The eddy covariance system was deployed from JD 205 until JD 289, 2000. Fluctuations of the vertical and horizontal wind speed and temperature were measured at 10 Hz using a (three-dimensional) sonic anemometer–thermometer (Gill R3, Gill Inc.). The CO_2 and H_2O vapor fluctuations were measured at the same response interval that winds were measured using an open-path infrared gas analyzer (IRGA) designed by NOAA/ATDD (Auble and Meyers, 1992). The sensors were mounted approximately 2.5 m above the ground. The high-frequency data (10 Hz) were recalculated and stored on the computer hard drive at 30-min intervals. Net CO_2, H_2O vapor and energy fluxes were computed using software designed by Tilden Meyers (National Oceanic and Atmospheric Association) and modified by Joe Verfaillie (San Diego State University).

The local meteorological conditions were recorded continuously along with the eddy covariance data. These data were measured every 10 s and averaged over a 30 min period, using a datalogger (model CR 21X, Campbell Scientific Inc., Ogden, UT). Air temperature and relative humidity were measured using a ventilated psychrometer mounted at a height of 1.7 m above the soil surface. Soil temperatures in elevated and depressed microhabitats were measured using t-type thermocouples at depths of 0, 5 and 10 cm. Net radiation (R_n) was measured using a net radiometer (model Q-6, REBS, Seattle, WA) at a height of 1 m above the ground. Soil heat flux (G) was determined using two soil heat flux plates (model HFT-1, REBS) installed in elevated and depressed microhabitats at a depth of 1 cm. Photosynthetically active radiation (*PAR*) was measured using a quantum sensor (model LI-190SB, LI COR Inc.). Diurnal sums of precipitation were measured using a plastic rain bucket.

The relative humidity and air temperature collected as part of the meteorological station data was used to calibrate the open-path IRGA response to water vapor content every 7 d during the entire field season. To estimate the calibration coefficients, 30-min averages of H_2O voltage output of the IRGA versus the corresponding 30-min average H_2O concentrations for a particular 7-d period were plotted. These concentrations were calculated using air relative humidity and temperature values. Three reference gases with known CO_2 concentrations (364, 395 and 435 $\pm$ 3 ppm) were used to calibrate the IRGA CO_2 channel under laboratory conditions and on a weekly basis in the field.

As the fluctuations in both CO_2 and H_2O vapor were measured *in situ,* flux estimates obtained from the eddy covariance system were corrected for simultaneous fluctuations in both sensible heat flux and H_2O vapor (Webb et al., 1980). Normally the corrections were -40 to -60% for CO_2 flux in summer and 20 to 40% for CO_2 flux in fall. The latent heat flux (L_e) was calculated using H_2O vapor values while sensible heat from the sonic temperature data. For diurnal estimates, the 30-min eddy flux data were integrated over 24-h intervals.

The comprehensive analysis of energy fluxes is beyond the scope of this paper. Nevertheless, closure of energy balance ($H+L_e = R_n-G$) is an important indication of system performance (Baldocchi et al., 1988; Lafleur, 1999). In our case, the energy closure could be characterized by the following equations: $(H + L_e) = 0.84\ (R_n - G) + 7.6\ (r^2 = 0.84)$ for 30-min data intervals and $(H + L_e) = 0.93\ (R_n - G) + 4.8\ (r^2 = 0.86)$ for diurnal values. With 30-minute average energy closures of 84%, and diurnal energy closures of 93%, we may consider the energy closure and system performance as satisfactory.

The height of the micrometeorological sensors at 2.5 m above ground corresponds to the low vegetation stature (20–30 cm) and smooth microtopography of the footprint. As in many other analogous micrometeorological studies in tundra, the variation of CO_2 storage in the air column beneath the eddy covariance instrumentation in our case may be neglected (Harazono et al., 1998; Vourlitis and Oechel, 1997; Williams et al., 2000), and a measured CO_2 flux can stand for the net ecosystem exchange (*NEE*).

The second method for CO_2 flux estimation we used was a well known chamber technique in combination with a closed-path analyzer (Vourlitis et al., 1993). We used a portable infrared CO_2 analyser (LI-6200LiCor, Lincoln NE, USA) and an acrylic cubic transparent cuvette (42 cm base) connected to the analyzer. Six stationary sample plots were established in the most representative ecosystems (mesic upland and wet lowland). Diurnal measurements were repeated weekly at

permanent sampling points. In total, 13 diurnal measurements were performed during the period JD 216–286 (2000) (Zamolodchikov et al., 2000a).

Soil moisture, thaw depth and water table were measured every 7 d along eight permanent transects, following the wind-rose directions with the eddy tower in the center. Each transect was 100 m long with permanent sampling points at every 10 m marked by flags. Depth of thaw was determined by inserting a steel rod near each sampling point (with three random replications) until permafrost was reached. The water table was measured using permanent water wells (two per every transect), 5 cm in diameter each, passing through the active layer. Volumetric soil moisture was estimated by measuring dielectric resistance in the topmost 7 cm of the soil organic horizon. We used a Vitel portable probe (*Hydra soil moisture probe user's manual, Version 1.2,* 1994) at the same sample points where thaw depth was measured. The moisture probe was calibrated gravimetrically on 185 volumetric soil samples taken from different ecosystems and organic/mineral horizons with varying moisture content. These calibrations resulted in the following polynomial regressions, characteristic for the local soils:

$$SM = -2.47 + 2.80E - 0.0432E^2 + 0.000279E^3,$$
$$r^2 = 0.947,\ SE = 7.3,\ n = 185, \qquad (1)$$

where SM is a volumetric soil moisture (%) and E is a real dielectric constant.

A full diurnal data set for a sampling day included 240 measurements of thaw depth, 240 measurements of soil moisture and 16 measurements of water table.

Coefficients for the non-linear equations were calculated using the software procedures of non-linear regression analysis in STATISTICA for Windows, Release 5.0, StatSoft, Inc.

3. Results

3.1. Weather and soil conditions during the period of observations

Mean air temperatures at the Lavrentiya site in August (JD 214–244) and September (JD 245–274) 2000 were 6.5 and 2.2 °C, respectively. The corresponding monthly sums of rainfall were 93 and 97 mm. Mean diurnal air temperature varied around 6 °C in summer, with a following gradual decrease to −3 °C near JD 288 (Fig. 1). Along with a general descending

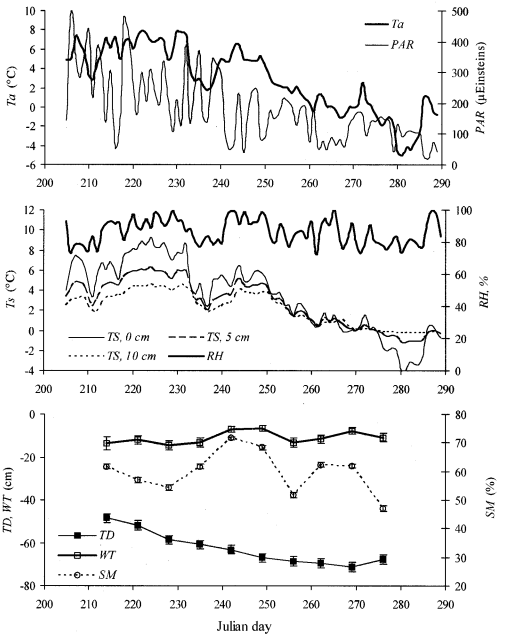

Fig. 1. Seasonal dynamics of mean daily temperature (T_a), mean daily photosynthetically active radiation (*PAR*), mean daily soil temperatures at 0, 5 and 10 cm (T_{s0}, T_{s5}, T_{s10}), relative air humidity (*RH*), thaw depth (*TD*), position of water table (*WT*) and volumetric soil moisture in 7 cm topmost layer (*SM*). Data for *TD*, *WT* and *SM* are means ± 1 *SE*, $n = 16$ (*WT*) or 240 (*TD*, *WT*).

trend during the sampling period, the diurnal *PAR* exhibited considerable intra-seasonal variation. The coefficient of variation (*CV*) of mean diurnal *PAR* for the period JD 205–244 was 0.47, while the *CV* of mean diurnal air temperature for the same period was only 0.28.

Seasonal variations of soil temperatures were closely correlated with air temperature ($r = 0.98$, 0.96 and 0.92 for the depths 0, 5 and 10 cm, respectively). Air and soil temperatures never exceeded 0 °C after JD 275.

The mean thaw depth was measured at 49 cm at the beginning of the study. This value gradually increased to a maximum of 71 cm (JD 269) and then decreased to 68 cm by JD 276 due to the beginning of a frost period. During the field season volumetric soil moisture in the topmost layer (7 cm) varied within the range 47–71% (mean 60%). The water table position varied from 7 to 15 cm below the soil surface (mean 11 cm). Soil moisture and water table position were positively correlated ($r = 0.60$, $P < 0.01$) (Fig. 1).

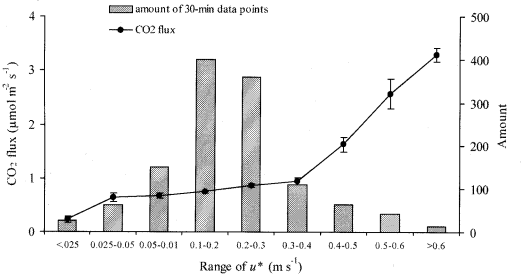

Fig. 2. Distribution of night-time 30-min intervals within the range of friction velocity (u^*) and corresponding mean CO_2 fluxes. Flux data are means ± 1 standard errors (*SE*), *n* varies from 14 to 400.

3.2. *Night-time NEE*

A well known uncertainty of the eddy covariance technique is underestimation of CO_2 flux in the night-time due to low wind speed and insufficient air turbulence (Goulden et al., 1996; Lafleur, 1999). A common practice is to identify the threshold friction velocity (u_c^*), beyond which flux seems to level off, and to replace the flux during periods with $u^* < u_c^*$ by the flux estimated by temperature functions, obtained during well mixed, windy periods. According to our data, the distribution of night-time *NEE* (*PAR* < 10 μ einsteins) mean values by u^* range bins demonstrate a considerable decrease of the flux at $u^* < 0.025$ m s^{-1} (Fig. 2). In the range $0.025 < u^* < 0.4$ night-time *NEE* is rather constant, whereas under greater friction velocities, CO_2 flux rapidly increased. Moreover, the sum of $(H + L_e)$ values at these friction velocities considerably exceeded the corresponding values of $(R_n - G)$, sometimes by a factor of ten. Because this situation did not meet the energy balance criterion of the optimal method performance, we excluded data with u^* values more than 0.4 m s^{-1}.

Notably, the research site was rather windy during the period of observations, with a mean horizontal wind speed (u) of 4.4 m s^{-1}. Friction velocity was closely correlated with u: $u^* = 0.054u + 0.0168$, $r^2 = 0.91$. On average, the lower threshold of friction velocity (0.025 m s^{-1}) corresponded to the horizontal wind speed of 1 m s^{-1}, whereas its upper threshold (0.4 m s^{-1}) corresponded to the wind speed of 7 m s^{-1}.

The rate of night-time *NEE* is equal to ecosystem night-time respiration (*ER*), where temperature is known as the main controlling factor. In order to find the temperature dependence of night-time *NEE* we used the exponential equation of van't Hoff (Lloyd and Taylor, 1994):

$$R = R_0 \exp(kT), \tag{2}$$

where T is temperature, R_0 is the basal rate of respiration, and k is a temperature sensitivity coefficient. Of the temperatures monitored, soil temperature at a depth of 5 cm (T_{s5}) demonstrated the best correlation with night-time *NEE* (Fig. 3). The equation

$$NEE_{night} = 0.544 \exp(0.180 T_{s5}) \tag{3}$$

explains 44.2% of the night-time *NEE* ($n = 1190$) variance, which is considered a good correspondence for results obtained by eddy covariance technique (Lafleur, 1999).

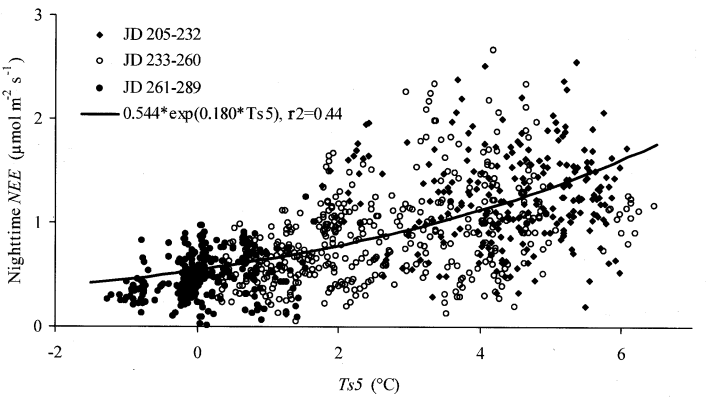

Fig. 3. Night-time *NEE* vs. soil temperature at 5 cm depth.

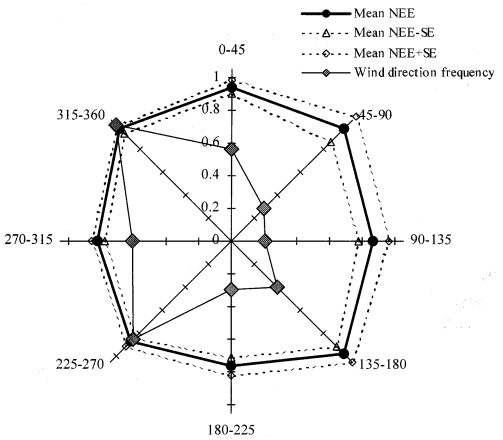

Fig. 4. Mean night-time *NEE* by eight 45° sectors of wind directions and the wind rose at the studied site for the period of observations.

In order to estimate the surface roughness of the instrumentation footprint, the night-time CO_2 flux 30-min data were separated by eight 45° wind sectors. Flux values were not considered if the corresponding u^* values were outside the acceptable range indicated above. No significant differences between mean wind sector night-time *NEE* fluxes were found (Fig. 4), which advocate for the homogeneity of the instrumentation footprint. The predominant wind directions were 225–270° and 315–360°, as 44% of all data fell within these ranges.

3.3. *Estimation of gross primary production*

Daytime *NEE* is the difference between ecosystem respiration (*ER*) and gross primary production (*GPP*). If the night-time *NEE*/soil temperature relationship is also applicable for the daytime, we can estimate daytime *GPP* flux. An independent closed-chamber method provided an opportunity to validate this assumption using available *ER* data. Analysis shows that daytime and night-time *ER* rates are similar, as are the approximated temperature dependencies (Fig. 5). Hence we can apply the regression (3) that was found using eddy covariance techniques to partition *ER* and *GPP* fluxes during the daytime.

When calculating *GPP* fluxes, only the 30-min data obtained under friction velocities within the $0.025 < u^* < 0.4$ range were used. Daytime (i.e. $PAR > 10$ μeinsteins) dynamics of ecosystem respiration were calculated using known soil temperatures at 5 cm depth and eq. (3), and gross primary production estimated as $GPP = ER - NEE$. A value of *NEE* is positive if the ecosystem functions as a source of CO_2 to the atmosphere, and negative when it functions as a sink.

PAR is well known as a primary control of *GPP* at a daily timescale, and this relationship is hyperbolic (Monsi and Saeki, 1953):

$$GPP = a_1 a_2 \times PAR/(a_1 \times PAR + a_2), \quad (4)$$

where a_1 is an initial slope and a_2 is a plateau of the light curve.

In general, our source data correspond to eq. (4) (Fig. 6). Nevertheless, a preliminary approximation of *GPP* over different observation periods (Fig. 6) indicates that parameter a_1 linearly decreased as the season progressed, i.e. it was JD-dependent. Data obtained by the independent chamber method demonstrated the same result. Hence, the Julian day (JD) was introduced

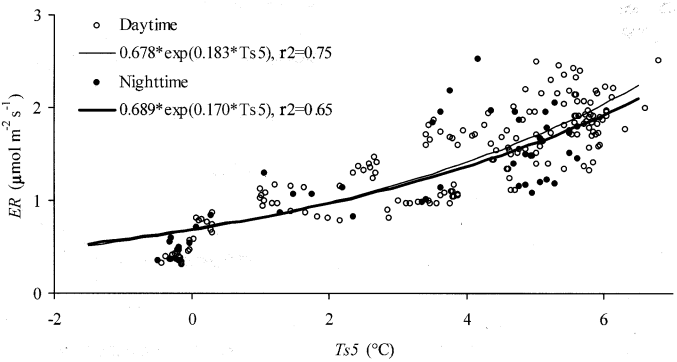

Fig. 5. Ecosystem respiration (*ER*) vs. soil temperature at 5 cm depth in day- and night-time. *ER* data are obtained by a closed chamber technique.

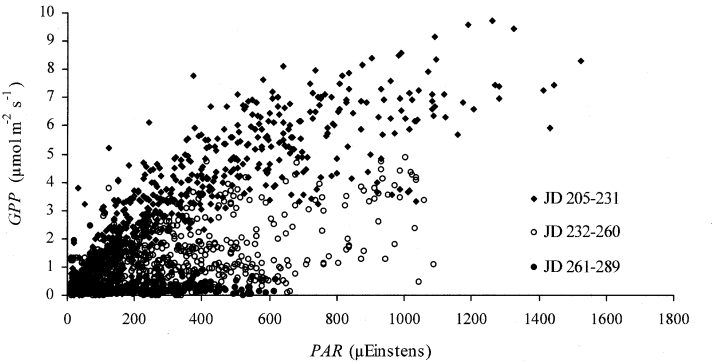

Fig. 6. Relationship between gross primary production (*GPP*) and *PAR*.

into the eq. (4) as a new factor:

$$GPP = (d_1 \times JD + d_2)a_1a_2 \times PAR/(a_1PAR + a_2), \quad (5)$$

where a_1 is an initial slope, a_2 is a plateau of a light curve, and d_1 and d_2 are JD parameters.

An approximation of the parameters of eq. (5) has shown a good correspondence with source data:

$$GPP = (-0.704 \times JD + 192) \times 0.000438 \times 0.263 \times PAR/(0.000438 \times PAR + 0.263),$$
$$r^2 = 0.84, n = 1834. \quad (6)$$

Use of air and soil temperatures instead of *JD* in eq. (5) resulted in poor coefficients of determination.

3.4. *Diurnal patterns of CO_2 fluxes*

In eddy covariance measurements, it is necessary to compensate for missing *NEE* flux data. During the period of observations, 4080 30-min data points were obtained overall. Some of the data were later rejected due to maintenance or instrumentation failure (320 points, or 7.8%), exceeding of the threshold values of friction velocity (640 points, or 15.7%), and other reasons (63 points, or 1.5%). To substitute for missing *NEE* data at night-time ($PAR < 10$ μ einsteins) we used eq. (3). To fill missing daytime data, the *ER* flux was estimated by eq. (3), *GPP* by eq. (6), and *NEE* was then calculated as $GPP - ER$. The observation period could be conditionally subdivided into four phenological stages: (i) active plant growth (JD 205–223); (ii) vascular plants leaf senescence (JD 224–244); (iii) leaf degradation and litter fall (JD 244–264); and (iv) soil freezing at the surface (JD 265–289). Diurnal dynamics of *NEE*, *ER* and *GPP* in the typical tundra ecosystems was considerably different depending on the particular period. Period (i) was characterized by a negative diurnal *NEE* (i.e. a CO_2 sink), with a mean daily carbon uptake of 4.4 μmol m^{-2} s^{-1} (Fig. 7A). Active photosynthesis of vascular plants was a major contributing factor for the carbon sink in this period. Mean daily rate of *ER* was about 1.4 μmol m^{-2} s^{-1}. During period (ii), the pattern of daily CO_2 dynamics was the same in general, but the mean duration of a daily carbon sink decreased from 13 to 11 h and the mean daily maximum rate was reduced more than 50% to 2.3 μmol m^{-2} s^{-1} (Fig. 7B). Mean daily rate of *ER* slightly decreased to 1.3 μmol m^{-2} s^{-1}. During period (iii), the system was a sink for CO_2 only 3 h of the day (Fig. 7C), and was rather negligible (0.1 μmol m^{-2} s^{-1}). During period (iv), the daytime emission of CO_2 (0.43 μmol m^{-2} s^{-1}) was even greater then at the night-time (0.38 μmol m^{-2} s^{-1}) (Fig. 7D). Nevertheless, the rate of *GPP* during this period was still significant (0.17 μmol m^{-2} s^{-1}). The chamber measurements also registered non-zero rates of *GPP* fluxes until the very end of measurements on JD 286, with an average rate of *GPP* of 0.22 μmol m^{-2} s^{-1} at this time. This was probably due primarily to photosynthetic activity of mosses, lichens and evergreen vascular plants.

The closed-chamber method provides an opportunity to compare eddy-based estimates of carbon fluxes with our independent estimate. The estimates of *NEE* by these two methods correspond well (Fig. 8A):

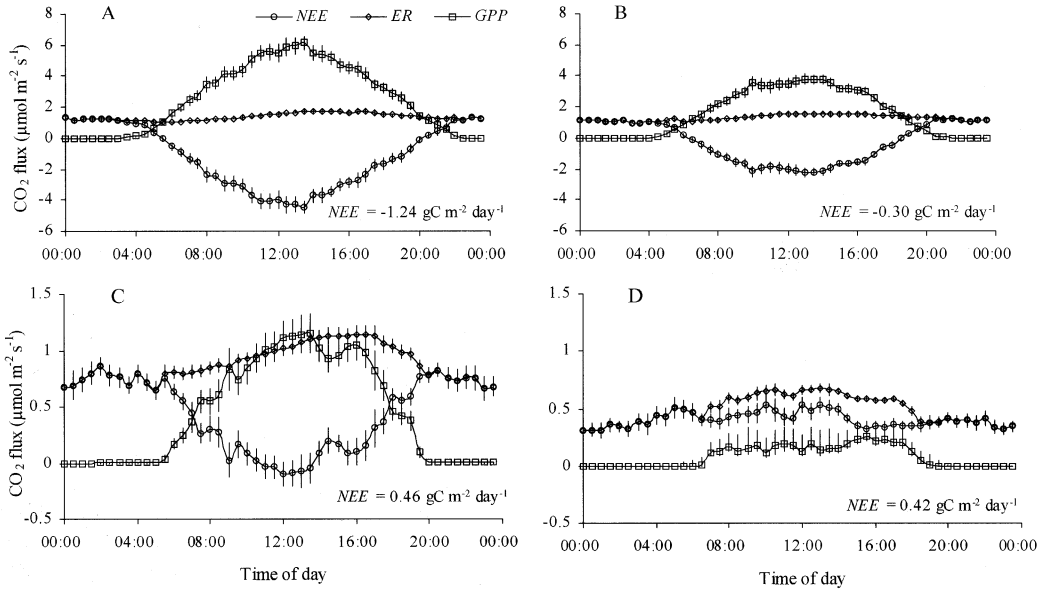

Fig. 7. Averaged eddy-based diurnal dynamics of net ecosystem exchange ($NEE = ER - GPP$), ecosystem respiration (ER) and gross primary production (GPP) for the periods: (A) JD 205–223; (B) JD 224–244; (C) JD 244–264; (D) JD 264–289. Data are means ± 1 SE; n are from 19 to 25. Negative NEE rate means a carbon sink to ecosystem, positive - means a carbon source.

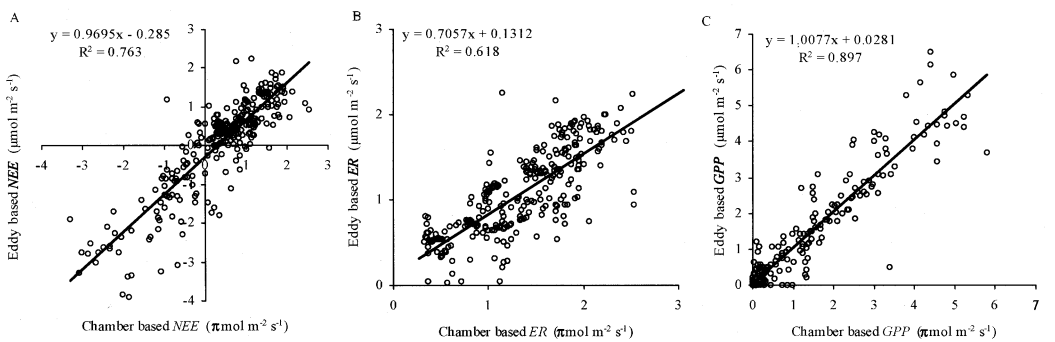

Fig. 8. Eddy-vs. chamber-based fluxes of net ecosystem exchange (NEE, A), ecosystem respiration (ER, B) and gross primary production (GPP, C).

$NEE_{eddy} = 0.97 \times NEE_{chamber} - 0.29$, $r^2 = 0.76$, $n = 280$. However, the negative intercept in this equation indicates that NEE_{eddy} estimates shifted to CO_2 sink at 0.29 μmol m^{-2} s^{-1}, as compared to $NEE_{chamber}$. The estimates of ER by these methods do not correspond well (Fig. 8B): $ER_{eddy} = 0.71 \times ER_{chamber} + 0.13$, $r^2 = 0.62$, $n = 280$. Despite the intercept of 0.13 μmol m^{-2} s^{-1}, the difference between the two estimates is almost 30%. In contrast, the correspondence between GPP estimates by the two methods is excellent (Fig. 8C): $GPP_{eddy} = 1.01 \times GPP_{chamber} + 0.03$, $r^2 = 0.90$, $n = 280$. Hence, in this study, we may conclude that NEE and, especially, GPP estimates by closed chamber and eddy covariance techniques are comparable, whereas ER fluxes are a source of uncertainty.

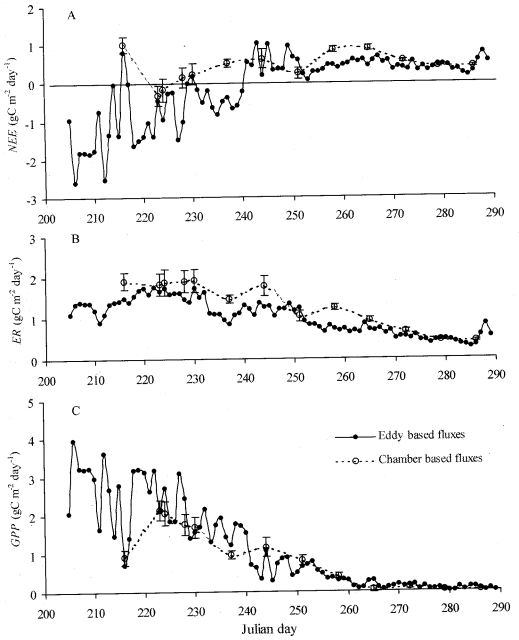

Fig. 9. Seasonal dynamics of eddy- and chamber-based daily integrated rates of net ecosystem exchange (*NEE*, A), ecosystem respiration (*ER*, B) and gross primary production (*GPP*, C) at Lavrentiya site (field season of 2000). The chamber-based data are means ± 1 *SE*, $n = 6$.

3.5. *Seasonal dynamics and controls of net ecosystem exchange*

Seasonal dynamics of daily integrated *NEE* values were highly variable ($CV = 1.83$) (Fig. 9A). Nevertheless, some seasonal trends and regularities were found. From JD 205–211, maximum rates of CO_2 sink were observed; from JD 213–240, *NEE* gradually approached zero; from JD 240–250, maximum CO_2 emission to the atmosphere was recorded.

Mean diurnal rates of *ER* (Fig. 9B) were not as variable ($CV = 0.42$). Maximum *ER* fluxes (up to 1.8 gC m^{-2} d^{-1}) were observed in the period of JD 219–232. Then *ER* diurnal values gradually decreased to 0.3 gC m^{-2} day^{-1} by the end of the period of observations (JD 282–286). A noticeable rise of *ER* rate at the end of observations was due to some warming during the last 3 d (Fig. 1).

Mean diurnal rates of *GPP* (Fig. 9C) were more variable than *ER* ($CV = 1.0$). A seasonal trend was well expressed: from JD 205–260, the rate of *GPP* decreased from 4.0 gC m^{-2} d^{-1} to 0.2 gC m^{-2} d^{-1}. This rate was almost constant until the end of observations on JD 289.

During the period of observations, the CO_2 budget in a typical tundra landscape was estimated as a weak carbon sink, with a *NEE* rate of −10.2 gC m^{-2}, *ER* rate of 85.5 gC m^{-2}, and *GPP* rate of 95.7 gC m^{-2}. Between JD 205 and 240, the studied ecosystems were primarily acting as a carbon sink and they sequestered 32.1 gC m^{-2} ($NEE = ER - GPP = 49.6 - 81.7$ gC m^{-2}). Between JD 241 and 289, the tundra emitted to the atmosphere 21.9 gC m^{-2} ($NEE = ER - GPP = 35.9 - 14.0$ gC m^{-2}).

Daily mean carbon dioxide fluxes were compared only for the days when both chamber- and eddy-based methods were in use. Seasonal changes of chamber- and eddy-based mean diurnal rates of *NEE* were rather similar ($r = 0.73$, $P = 0.004$) (Fig. 9A). The difference between seasonal means of *NEE* fluxes estimated by both methods was statistically insignificant (paired t-test, $P = 0.22$). Seasonal changes of mean diurnal *ER* fluxes estimated by both methods were well correlated ($r = 0.91$, $P = 0.002$) (Fig. 9B). Nevertheless mean seasonal rates of *ER* were significantly different (paired t-test, $P < 0.01$). Diurnal rates of *GPP* from chamber and eddy measurements were the most synchronous ($r = 0.96$, $P < 0.01$) (Fig. 9C), with almost equal seasonal means (paired t-test, $P = 0.27$).

As mentioned above, the *NEE* values included in this analysis were 75% observed and 25% were modeled based on temperature/*ER* and *PAR*/*GPP* dependencies. To check for the influence of the modeling on the final result, we used linear interpolation, which is the most common method for gap-filling data. Figure 10 shows that both methods resulted in similar values of cumulated *NEE*; the final seasonal value after the modeling was estimated at −10.2 gC m^{-2} and −11.3 gC m^{-2} after linear interpolation.

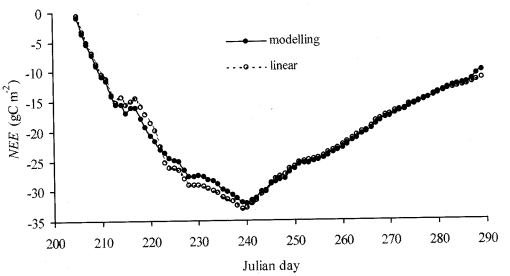

Fig. 10. Cumulated *NEE*, estimated by two methods of missing data in-filling: (1) process-based modelling and (2) linear interpolations.

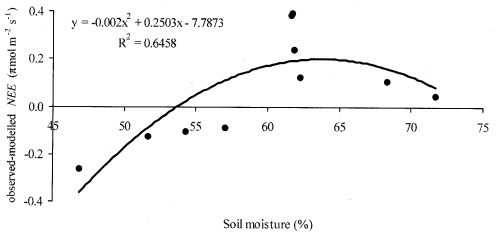

Fig. 11. A difference between observed and modeled night-time *NEE* fluxes vs. volumetric soil moisture.

3.6. *Other controls of NEE*

It was shown that soil temperature was a leading factor determining the dynamics of night-time *NEE* and *ER*. Other potential environmental controls of these fluxes should be considered, namely, depth of active soil layer, soil moisture and water table position. As these controls were measured weekly, only mean diurnal fluxes of CO_2 were used in the analysis. Due to the significant correlation between thaw depth and soil temperature ($r = 0.77$, $P < 0.05$), and between soil moisture and water table position ($r = 0.60$, $P < 0.05$), we did not use these data in our multiple statistical analysis.

An analysis of the residual variation of night-time *NEE* after approximation of the flux by soil temperature factor was made. Firstly a mean diurnal night-time *NEE* rate (only observed data were included) and a corresponding soil temperature at 5 cm depth were calculated. Then a regression for mean diurnal values of night-time *NEE* and soil temperature was built ($NEE_{night} = 0.515 \exp(0.186 T_{s5})$, $r^2 = 0.54$, $n = 85$). We then used this equation to estimate a modeled values of night-time *NEE* for the days of the factors measurement, and calculated a difference between the modeled and observed night-time *NEE* flux rates.

The analysis shows that soil moisture was the only factor which demonstrated a significant correlation with that difference ($r = 0.63$, $P < 0.05$, $n = 10$; see also Fig. 11).

4. Discussion

The application of micrometeorological methods to measure CO_2 flux in the atmosphere has several obvious advantages. The most important features are that micrometeorological models provide continuous measurements and landscape-integrated *in situ* estimates. This approach also minimizes the impact on studied habitats. Nevertheless, the micrometeorological theory upon which the eddy covariance technique is based, has several important assumptions, not always realistic *in situ* (Baldocchi et al., 1988). Long-term micrometeorological studies face many additional problems. One is that turbulent CO_2 flux approaches zero as the level of turbulence, measured by the friction velocity, drops to zero (Goulden et al., 1996). Low friction velocity may result in considerable underestimation of emission fluxes. Many studies estimate a threshold value u_c^*, and CO_2 flux rates observed under $u^* < u_c^*$ are then subject to different corrections. u_c^* values vary from site to site within the range 0.1–0.4 m s^{-1}, depending on the height of micrometeorological instrumentation and plant canopy (Blanken et al., 1988). In our study, the night-time CO_2 flux considerably decreased at $u^* < 0.025$ m s^{-1}, which is no doubt one of the lowest estimates of u_c^* recorded in literature. Unfortunately we did not find any published u_c^* values for Arctic regions.

Some authors (Rayment and Jarvis, 2000) consider a CO_2 flux from the soil surface to be dependent on air turbulence. Variations in barometric pressure at the ground surface are correlated with turbulence intensity (Shaw and Zhang, 1992), and they are responsible for the transfer of CO_2 between soil and the atmosphere (the so called "pressure pumping effect"). In this case, u_c^* correction may result in overestimation of emission fluxes. The results of this study (Fig. 2) show that in the range of $0.025 < u^* < 0.4$ m s^{-1} the values of night-time *NEE* are gradually increase from 0.64 to 0.94 μmol m^{-2} s^{-1}. This may be due to the effect of turbulence on CO_2 exchange between soil and the atmosphere.

A strong increase of night-time *NEE* emissions under $u^* > 0.4$ m s^{-1} is also of interest (Fig. 2). Similar results were obtained in Arctic coastal tundra (Barrow, Alaska) during winter and thawing period (Harazono et al., 2001). In this study, a steep rise of CO_2 flux rates was observed under $u^* > 0.3$ m s^{-1} and a horizontal wind speed $u > 8$ m s^{-1}. In the cited paper this effect is explained by blizzing of CO_2 from the snowpack. We may also accept the pressure pumping effect as an explanation of the phenomena, but there are alternative possibilities. First, there is a very poor energy closure under high u^* rates [$(L_e + H)$ was 2.5 times greater than $(R_n - G)$]. The second alternative assumes that a CO_2 exchange between soil and the atmosphere under continuous pressure pumping should come to equilibrium with CO_2 production in soil. Hence we may expect a gradual decrease of CO_2 fluxes under continuously

high u^*. However, in our case this was not found even after several days under high u^* values (JD 279–281), so this forced us to take the upper threshold value of u^* into consideration. A more detailed analysis of the phenomena needs a monitoring of CO_2 storage in soil and its dynamics under high rates of u and u^*.

The night-time *NEE*/soil temperature dependency was successfully applied for extrapolation of missing flux data during the entire period of observations in this study. The use of constant values of basal rate (R_0) and temperature sensitivity coefficient (k) during a warm period is characteristic for model interpretations of micrometeorological measurements in Arctic ecosystems (Oechel et al., 2000b; Soegaard and Nordstroem, 1999). In contrast, in forest ecosystems R_0 and k were found to be highly specific to different seasons of the year (Rayment and Jarvis, 2000).

A seasonal dependency of the *GPP/PAR* relationship used in this study was a major feature. An addition of a Julian Day parameter to eq. (5) resulted in high coefficient of determination of the source data ($r^2 = 0.84$). Functionally, seasonal dynamics of the magnitude at light saturation in Arctic ecosystems depends on a state of development of the assimilation organs of vascular plants. The latter is usually characterized by leaf biomass, leaf area or *NDVI*. In different types of tundra the dynamics of *NDVI* demonstrates a sigmoidal pattern during vegetative season (Oechel et al., 2000b). As this study was conducted in the latter part of the growing season, i.e. during a decline of green phytomass storage, this explains the importance of Julian Day number in the final approximation.

Besides soil temperature, soil moisture was found to be the only other significant control of night-time *NEE* or *ER* in this study. Within the volumetric soil moisture range of 60–70%, the observed night-time *NEE* rates exceeded the flux values if modeled by soil temperature alone, i.e. this moisture range might be considered as optimal for the ecosystem carbon emission (Fig. 11). In general this follows the regularities known for carbon dioxide emission in Arctic and peat ecosystems. Despite the fact that soil/ecosystem respiration and CO_2 transport are potentially sensitive to a wide range of soil moisture, there is usually a plateau of maximum carbon emission under some intermediate moisture conditions, and any variation in soil moisture outside these conditions results in a decrease in carbon emissions (Hogg et al., 1992; Christensen et al., 1998; and others) due to suppression of a microbial respiration and vertical CO_2 transport in soil to some basal rate.

In this study, *PAR* was a significant control of *NEE* variations, which was not true for temperature owing to the local weather conditions during the period of measurements. Both temperature and *PAR* gradually decreased over the course of a season, whereas a variation of the diurnal *PAR* values was much greater than that of temperature. As compared to *ER*, this resulted in a greater variation of *GPP* values with corresponding changes in *NEE*. Note that this may not always be the case. In the summer seasons of 1995–96 in the north-east of the European tundra, the coefficient of variation of *GR* (0.4) exceeded that of *GPP* (0.2), and air temperature was found to be the key factor in *NEE* variations (Zamolodchikov et al., 2000a).

The long-term changes of *NEE* in the Arctic are believed to be driven mostly by temperature and local hydrology (precipitation, soil moisture and water table position) (Hobbie et al., 2000; Chapin et al., 2000; Oechel et al., 1995; 2000). *PAR*, which potentially can compensate for variation in other factors, possibly needs more attention. A decrease in rainfall may result in a corresponding reduction of soil moisture, which can activate *ER* (an increase of CO_2 source). On the other hand, a decrease of precipitation is normally connected with a decline in cloudiness and promotes a rise of *PAR* and *GPP* (an increase of CO_2 sink).

Estimation of energy balance closure is by no means one of the most widespread methods of evaluating the eddy covariance technique performance (Baldocchi et al., 1997; Jarvis et al., 1997; Lafleur, 1999), assuming that the fluxes of all other constituents are being measured adequately. Due to a low canopy stature tundra vegetation provides an independent option to evaluate the performance of CO_2 flux measurements using a chamber-based method. Our data show that these methods can provide comparable results, which is true for both diurnal and seasonal dynamics of *NEE*. Despite the finding that seasonal *NEE* fluxes estimated by these methods did not differ statistically, the analogous *ER* estimates were significantly different (Figs. 8 and 9). In contrast, the observed *GPP* fluxes obtained by chamber measurements and the modeled estimates of *GPP* by eddy covariance measurements were almost identical. We believe that the differences in *ER* estimates are mainly due to the different scale of these methods. The chamber measurements were conducted at six sample plots about 1 m^2 in total, whereas the footprint of eddy covariance instrumentation was at least several thousand square metres, representing a wider range of tundra microhabitats. Nevertheless, we consider these methods to give comparable results

in our case despite the existing differences in spatial resolution and accuracy. Mean seasonal estimates of *NEE* vary by different chamber plots between −0.4 and 0.83 gC m^{-2} d^{-1}. The average eddy-based estimate of *NEE* for the same days of measurements fits this range quite well (0.23 gC m^{-2} d^{-1}). These results are also consistent with earlier CO_2 exchange measurements in Russian tundra, which were based on chamber measurements only (Zamolodchikov and Karelin, 2001).

Seasonal dynamics of CO_2 surface fluxes demonstrate the same patterns in different tundra ecosystems and regions (Oechel et al., 2000; Vourlitis and Oechel, 1997; Zamolodchikov et al., 2000b; Zimov et al., 1993; 1996). This includes some characteristic extremes: a midwinter minimum of carbon emission, spring and autumn maximums of emission, and midsummer maximum of carbon sink. The period of field observations in this study covered the maximum summer sink and autumnal emission only (JD 205–289). These extreme rates were estimated at 1.72 and 0.48 gC m^{-2} d^{-1}, respectively. During the period JD 205–240 (2000) when a carbon sink pattern was predominant, the observed landscape locality of typical Far East tundra sequestered 32 gC m^{-2} from the atmosphere. We consider this value an estimate of maximum CO_2 sink at the studied site during the warm season of 2000. The value is within the range of variation of other known eddy-based warm season estimates of *NEE* in Arctic regions. In the mid 1990s, coastal wet sedge ecosystems in Alaska were functioning as a low summer carbon sink at 20 gC m^{-2} (Vourlitis and Oechel, 1997) but demonstrated a much greater summer sink activity in 1999 (120 gC m^{-2}) (Oechel et al., 2000a). In 1995 a wet sedge tundra of inland Alaska was a carbon sink of 75 gC m^{-2} (Harazono et al., 1998). In another example a high Arctic fen in Greenland was a carbon sink at 96 gC m^{-2} (Soegaard and Nordstroem, 1999).

The analysis of recent trends of temperature and precipitation shows that climatic conditions in the Chukotskiy Peninsula in the 1990s were rather stable (Zukert and Zamolodchikov, 1997), as compared to the North Slope of Alaska. We believe that the observed carbon exchange rates of local tundra in the Chukotskiy Peninsula are characteristic for this state of climate. Another way to check for this point is an application of the general regression-based model of carbon fluxes in tundra (Zamolodchikov and Karelin, 2001). After the model was tuned to the weather data of the Chukotskiy region during the 1990s, the total summer sink was estimated at 63 gC m^{-2}. This modeled estimate corresponds quite well to the observed carbon sink of 32 gC m^{-2} in this study during the second part of the growing season.

5. Acknowledgments

The research was supported by the National Science Foundation (USA), Arctic Systems Science, Land-Atmosphere-Ice-Interactions Program (OPP-9216109).

We are grateful to Glenn Sheehan (Barrow Arctic Science Consortium, USA) and Gennady Zelenski ("Naukan" cooperative society, Lavrentiya, Russia) for logistical and financial support of the field research, and Rommel Zulueta (San Diego State University, San Diego, USA) for help in understanding the theory and practice of the eddy covariance technique. Thanks are also due to anonymous reviewers and editorial staff for help in preparing the manuscript.

REFERENCES

Auble, D. L. and Meyers, T. P. 1992. An open path, fast response infrared absorption gas analyzer for H_2O and CO_2. *Boundary-Layer Meteorol.* **59**, 243–256.

Baldocchi, D. D., Hicks, B. B. and Meyers, T. P. 1988. Measuring biosphere-atmosphere exchanges of biologically related gazes with micrometeorological methods. *Ecology* **65**, 1331–1340.

Baldocchi, D. D., Valentini, R., Running, S., Oechel, W. and Dahlman, R. 1996. Strategies for measuring and modelling of carbon dioxide and water vapour over terrestrial ecosystems. *Global Change Biol.* **2**, 159–168.

Baldocchi, D. D., Vogel, C. A. and Hall, B. 1997. Seasonal variation of energy and water exchange rates above and below a boreal jack pine forest canopy. *J. Geophys. Res.* **102**, 28 939–28 951.

Billings, W. D. 1987. Carbon balance of Alaskan tundra and taiga ecosystems: past, present and future. *Quaternary Sci. Revi.* **6**, 165–177.

Blanken, P. D., Black, T. A., Neumann, H. H., Den Hartog, G., Yang, P. C., Nesic, Z., Staebler, R., Chen, W. and Novak, M. D. 1998. Turbulent flux measurements above and below the overstory of a boreal aspen forest. *Boundary-Layer Meteorol.* **89**, 109–140.

Chapin, F. S. III, McGuire, A. D., Randerson, J., Pielke, R., Baldocchi, D., Hobbie, S. E., Roulet, N., Eugster, W., Kasischke, E., Rastetter, E. B., Zimov, S. A. and Running,

W. 2000. Arctic and boreal ecosystems of western North America as components of the climate system. *Global Change Biol.* **6** (Suppl. 1), 211–223.

Chapman, W. L. and Walsh, J. E. 1993. Recent variations of sea ice and air temperature in high latitudes. *Bull. Am. Meteorol. Soc.* **74**, 33–47.

Christensen, T. R., Jonasson, S., Michelsen, A., Callaghan, T. V. and Havstrom, M. 1998. Environmental controls on soil respiration in the Eurasian and Greenlandic Arctic. *J. Geophys. Res.* **103**, D22, 29 015–29 021.

Eugster, W., McFadden, J. P. and Chapin, F. S. III. 1997. A comparative approach to regional variation in surface fluxes using mobile eddy correlation towers. *Boundary-Layer Meteorol.* **85**, 293–307.

Goulden, M. L., Munger, J. W., Fan, S.-M., Daube, B. C. and Wofsy, S. C. 1996. Measurements of carbon sequestration by long term eddy covariance: Methods and a critical evaluation of accuracy. *Global Change Biol.* **2**, 169–182.

Harazono, Y., Mano, M., Yoshimoto, M., Vourlitis, G. L. and Oechel, W. C. 1998. CO_2 budget of inland Arctic tundra in Alaska, micrometeorological measurements and empirical evaluations. *Proceedings of 23rd Conference on Agricultural and Forest Meteorol, 2–6 November, 1998.* American Meteorological Society, 111–114.

Harazono, Y., Mano, M., Miyata, A., Zulueta, R. C. and Oechel, W. C. 2003. Inter-annual carbon dioxide uptake at wet sedge tundra ecosystem in the Arctic. *Tellus* **55B**, in press

Hobbie, S., Schimel, J., Trumbore, S. and Randerson, J. R. 2000. Controls over carbon storage and turnover in high-latitude soils. *Global Change Biol.* **6** (Suppl. 1), 196–210.

Hogg, E. H., Lieffers, V. J. and Wein, R. W. 1992. Potential carbon losses from peat profiles: effects of temperature, drought cycles, and fire. *Ecol. Appl.* **2**, 298–306.

Hydra soil moisture probe user's manual. Version 1.2. 1994. Vitel, Inc., Cahntilly, VA, 24 pp.

Jarvis, P. G., Massheder, J. M., Hale, S. E., Moncrieff, J. B., Rayment, M. and Scott, S. L. 1997. Seasonal variation on carbon dioxide, water vapor and energy exchanges of a boreal black spruce forest. *J. Geophys. Rese.* **102**, 28 953–28 966.

Lafleur, P. M. 1999. Growing season energy and CO_2 exchange at a subarctic boreal woodland. *J. Geophys. Res.* **104**, 9571–9580.

Lloyd, J. and Taylor, J. A. 1994. On the temperature dependence of soil respiration. *Funct. Ecol.* **8**, 315–323.

Kozhevnikov, J. P. and Zheleznov-Chukotskii, N. K. 1995. *Beringia: its history and evolution.* Moscow, Nauka, 383 pp (in Russian).

Melillo, J. M., McGuire, A. D., Kicklighter, D. W., Moore, B., Vorosmarty, C. J. and Schloss, A. L. 1993. Global climate change and terrestrial net primary production. *Nature* **363**, 234–240.

Miyata, A., Leuning, R., Denmead, O. T., Kim, J. and Harazono, Y. 2000. Carbon dioxide and methane fluxes from an intermittently flooded pady field. *Agric. For. Meteorol.* **2779**, 1–17.

Monsi, M. and Saeki, T. 1953. Uber den Lichtfaktor in den Pflanzengesellschaften und seine Bedeutung fur die Stoffproduction. *Jpn. J. Bot.* **14**, 22–56.

Oechel, W. C., Hastings, S. J., Jenkins, M., Riechers, G., Grulke, N. and Vourlitis, G. 1993. Recent change of Arctic tundra ecosystems from a carbon sink to a source. *Nature* **361**, 520–523.

Oechel, W. C. and Vourlitis, G. L. 1994. The effects of climate change on Arctic tundra ecosystems. *Trends Ecol. Evolut.* **9**, 324–329.

Oechel, W. C., Vourlitis, G. L., Hastings, S. J. and Bochkarev, S. A. 1995. Change in Arctic CO_2 flux over two decades: effects of climate change at Barrow, Alaska. *Ecol. Appl.* **5**, 846–855.

Oechel, W. C., Vourlitis, G. L., Hastings, S. J., Hinzman, L. and Kane, D. 2000a. Acclimation of ecosystem CO_2 exchange in the Alaskan Arctic in response to decadal warming. *Nature* **406**, 978–981.

Oechel, W. C., Vourlitis, G. L., Verfaillie, J. Crawford, T., Brooks, S., Dumas, E., Hope, A., Stow, D., Boynton, B., Nosov, V. and Zulueta, R. 2000b. A scaling approach for quantifying the net CO_2 flux of the Kuparuk river Basin, Alaska. *Global Change Biol.* **6** (Suppl. 1), 160–173.

Rayment, M. B and Jarvis, P. G. 2000. Temporal and spatial variation of soil CO_2 efflux in a Canadian boreal forest. *Soil Biol. Biochem.* **32**, 35–45.

Rannik, Ü., Aubinet, M., Kurbanmuradov, O., Sabelfeld, K. K., Markkanen, T. and Vesala, T. 2000. Footprint analysis for measurements over a heterogeneous forest. *Boundary-Layer Meteorol.* **97**, 137–166.

Shaw, R. H. and Zhang, X. J. 1992. Evidence of pressure-forced flow in forest. *Boundary-Layer Meteorol.* **58**, 273–288.

Soegaard, H. and Nordstroem, C. 1999. Carbon dioxide exchange in a high-arctic fen estimated by eddy covariance measurements and modelling. *Global Change Biol.* **5**, 547–562.

Scientific-applied reference book on climate of USSR. 1990. Issue 33. Magadan district. Leningrad, Gidrometeoizdat, 566 pp (In Russian).

Vourlitis, G. L., Oechel, W. C., Hastings, S. J. and Jenkins, M. A. 1993. A system for measuring in situ CO_2 and CH_4 flux in unmanaged ecosystems: an arctic example. *Funct. Ecol.* **7**, 369–379.

Vourlitis, G. L. and Oechel, W. C. 1997. Landscape-scale CO_2, H_2O vapour and energy flux of moist-wet coastal tundra ecosystems over two growing seasons. *J. Ecol.* **85**, 575–590.

Webb, E. K., Pearman, G. I. and Leuning, R. 1980. Corrections of flux measurements for density effects due to heat and water vapour transfer. *Q. J. R. Meteorol. Soc.* **106**, 85–100.

Williams, M., Eugster, W., Rastetter, E. B., McFadden, J. P. and Chapin, F. S. III. 2000. The controls on net ecosystem productivity along an Arctic transect: a model comparison with flux measurements. *Global Change Biol.* **6** (Suppl. 1), 116–126.

Zamolodchikov, D. G., Karelin, D. V. and Ivaschenko, A. I. 2000a. Sensitivity of tundra carbon balance to ambient

temperature. *Water, Air and Soil Pollution* **119**, 157–169.

Zamolodchikov, D. G., Lopes de Gerenu, V. O., Karelin, D. V., Ivaschenko, A. I. and Chestnykh, O. V. 2000b. Carbon emission by the southern tundra during cold seasons. *Docl. Biol. Sci.* **372**, 312–314.

Zamolodchikov, D. G. and Karelin, D. V. 2001. An empirical model of carbon fluxes in Russian tundra. *Global Change Biol.* **7**, 147–162.

Zimov, S. A., Zimova, G. M., Davidov, S. P., Davidova, A. I., Voropaev, Y. V., Voropaeva, Z. N., Prosiannikov, S. F., Prosiannikova, O. V., Semiletova, I. V. and Semiletov, I. P. 1993. Winter biotic activity and production of CO_2 in Siberian soils: A factor in greenhouse effect. *J. Geophys. Res.* **98**, 5017–5023.

Zimov, S. A., Semiletov, I. P., Davidov, S. P., Voropaev, Y. V., Prosiannikov, S. F., Chapin, M. C. and Chapin, F. C. III. 1996. Siberian CO_2 efflux in winter as a CO_2 source and cause of seasonality in atmospheric CO_2. *Climatic Change* **33**, 111–120.

Zimov, S. A., Davidov, S. P., Zimova, G. M., Davidova, A. I., Chapin, F. S. III, Chapin, M. C. and Reynolds, J. F. 1999. Contribution of disturbance to increasing seasonal amplitude of atmospheric CO_2. *Science* **284**, 1973–1976.

Zukert, N. V. and Zamolodchikov, D. G. 1997. Long-term trends of air temperature and precipitation in Russian tundra zone. *Meteorologiya i Gidrologiya (Meteorology and Hydrology)* **8**, 45–52 (in Russian).